An Ultra-Wideband Dielectric Rod Antenna Fed by a Planar Circular Slot

Mario Leib, *Student Member, IEEE*, Andreas Vollmer, and Wolfgang Menzel, *Fellow, IEEE*

***Abstract*—A novel ultra-wideband (UWB) dielectric rod antenna fed by a planar structure is presented. The planar structure consists of a circular slot antenna supplied by a dipole. This planar antenna excites the HE_{11} mode of an attached circular dielectric rod. Due to this combination, a broadband and low-dispersive overall antenna performance is achieved. Furthermore, an additional reflector at the backside of the antenna increases the directivity. With this configuration, a return loss better than 10 dB from 3.5 to 11.8 GHz is achieved with a nearly constant gain and a mean gain of 8.7 dBi. Beside the standard characterization, the system performance of the antenna is evaluated by means of the fidelity factor calculated from time-domain measurements and applying a UWB impulse generator.**

***Index Terms*—Antennas, dielectric antennas, directive antennas, ultra-wideband (UWB) antennas.**

I. Introduction

THE ultra-wideband (UWB) technology offers a vast bandwidth of 7.5 GHz at a center frequency of 6.85 GHz according to the Federal Communications Commission (FCC) regulations [1]. The resulting high range resolution of 3 cm brought up various novel sensing applications in different areas. Ground penetrating radars mainly investigated in the past for land-mine detection in the military sector [2], [3] became interesting for civilian applications like detection of trapped people [4] or nondestructive evaluation of concrete, pavements, and walls [5], [6]. Other industrial utilization of UWB can be found in tank level gauging in order to separate different liquid layers [7] and for material identification, e.g., to distinguish human tissue from wood on table saws for safety purposes [8]. Some products are already commercially available, e.g., a wall scanner for the analysis of building material.[1] In the medical environment, further emerging UWB applications are considered reaching from breast cancer detection [9], [10] and vital signs monitoring [11], [12] to tracking of inner organs for improved magnetic resonance tomography [13].

Directive UWB antennas are required for most of these applications. Beside the mandatory electrical characteristics like broadband matching, constant radiation pattern, uni-directionality, and a low dispersion, aspects like light weight, cost effectiveness, compactness, and ease of fabrication are important, in particular if an industrial product is targeted. Hence, planar antennas are often preferred. Tapered slot antennas (TSAs), especially the exponentially tapered Vivaldi antenna [14], show a broadband behavior and are used in many applications [12], [15], [16]. Frequently, they are applied in combination with antenna arrays due to their low lateral dimensions [17], [18]. However, this antenna type has an undesired broad radiation pattern in the H-plane, a low front-to-back ratio, and is mechanically instable. In contrast to this, stacked-patch antennas [19], [20] are robust, flat, and compact, but they achieve only a relative bandwidth of about 70% and cannot cope with the demanded value of 110%. Another idea is to place a reflector behind or beside an omnidirectional planar UWB antenna like a fat dipole or monopole. Thus, the gain of the antenna can be increased. The shortcoming is a decrease of the return loss at lower frequencies [21], a strong variation of the radiation pattern, and a bulky structure [22].

A more promising approach is to exploit dielectric rod antennas. In [23], a dielectric rod is placed around a Vivaldi antenna to get a similar beamwidth in both planes. This method circumvents the aforementioned drawbacks of the TSA; however, it is mechanically difficult to integrate the rod around the planar antenna while keeping a good return loss. An even more complicated structure is presented in [24]. In that paper, a half biconical dipole is combined with a dielectric rod antenna and a reflector. This combination leads to an outstanding electrical performance, but at the cost of a very sophisticated, and hence, expensive antenna manufacturing.

In this paper, a similar concept is proposed. Instead of a 3-D structure, a simple planar circular slot antenna is applied to feed a dielectric rod antenna. As will be shown, the antenna exhibits very good electrical properties in the frequency and time domain due to its traveling-wave characteristic, while keeping a simple fabrication and assembly. Since the antenna is fed by a planar structure, active components can be directly integrated on the feeding substrate giving the potential for a very compact overall system. Furthermore, the dielectric rod protects and insulates the sensor electronics. Such an arrangement could be beneficial for tank level gauging with chemically aggressive or conductive liquids.

In this paper, the design of the proposed antenna will be described in detail and the characteristics of the antenna will be

Manuscript received May 25, 2010; revised December 23, 2010; accepted January 08, 2011. Date of publication March 10, 2011; date of current version April 08, 2011. This work was supported by the German Research Foundation (DFG).

M. Leib is with EADS Deutschland GmbH, 89077 Ulm, Germany (e-mail: mario.leib@cassidian.com; mario.leib@ieee.org).

A. Vollmer is with Emitel AG, 89081 Ulm, Germany (e-mail: andreas.vollmer@ulm.emitel.de).

W. Menzel is with the Institute of Microwave Techniques, University of Ulm, 89081 Ulm, Germany (e-mail: wolfgang.menzel@uni-ulm.de).

Color versions of one or more of the figures in this paper are available online at http://ieeexplore.ieee.org.

Digital Object Identifier 10.1109/TMTT.2011.2114050

[1]Wallscanner D-tect 150, Bosch GmbH, Gerlingen, Germany, 2009. [Online]. Available: http://www.wallscanner.com

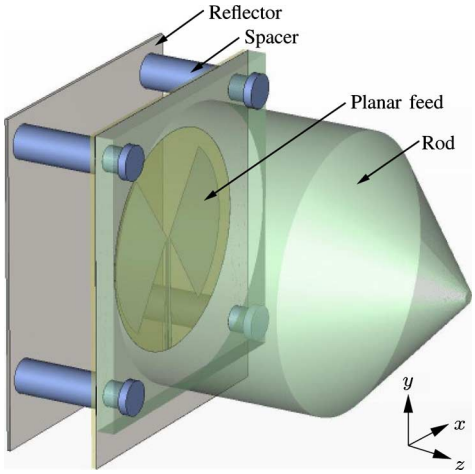

Fig. 1. Sketch of the proposed UWB antenna fed by a slot antenna. The rod and substrate are drawn semitransparent to show the planar feeding.

shown. A special focus will be on the antenna characterization in the time domain. Finally, the properties of the antenna will be compared to recent developments of alternative UWB antennas.

II. Basic Antenna Design

The basic antenna concept is the combination of a planar UWB antenna with a circular dielectric rod, where the planar antenna acts as feed for the rod antenna. For a unidirectional radiation pattern, a reflector is added at a certain distance behind the feeding element. In Fig. 1, the final structure including all three main components (planar UWB antenna, dielectric rod, metallic reflector) is sketched. The 3-D simulation software Microwave Studio [25] has been used for the complete antenna design.

For the planar UWB antenna, a differentially fed circular slot antenna is chosen [26], where a coplanar stripline feeds two open-circuited stubs (cf. Fig. 2). These stubs act as a broadband dipole and provide, together with the slot in the ground plane, a uniform radiation pattern over frequency. Hence, the dielectric rod is excited very uniformly. The differential feeding of the basic antenna avoids parasitic radiation by the feeding line or by cable currents [27]. In addition, the benefits of differential monolithic microwave integrated circuits (MMICs) can be exploited for a complete system, e.g., improved power supply rejection and less susceptibility to interferences. The dimensions of the planar antenna without the rod are designed to obtain a return loss better than 10 dB starting from 3 GHz. The simulated gain of the basic planar antenna is shown in Fig. 3. Within the FCC frequency range from 3.1 to 10.6 GHz the gain variation is ± 1.7 dB with a mean gain of 5.2 dBi.

Due to the field distribution within the slot antenna, the fundamental mode HE_{11} of the circular dielectric waveguide is predominantly excited. This hybrid mode possesses no cutoff frequency, and hence, provides an inherently broadband performance. The diameter of the dielectric waveguide is slightly larger than the feeding slot and is a compromise between single-mode operation and good field excitation by the planar feed. A linear taper at the open end of the dielectric radiator acts as

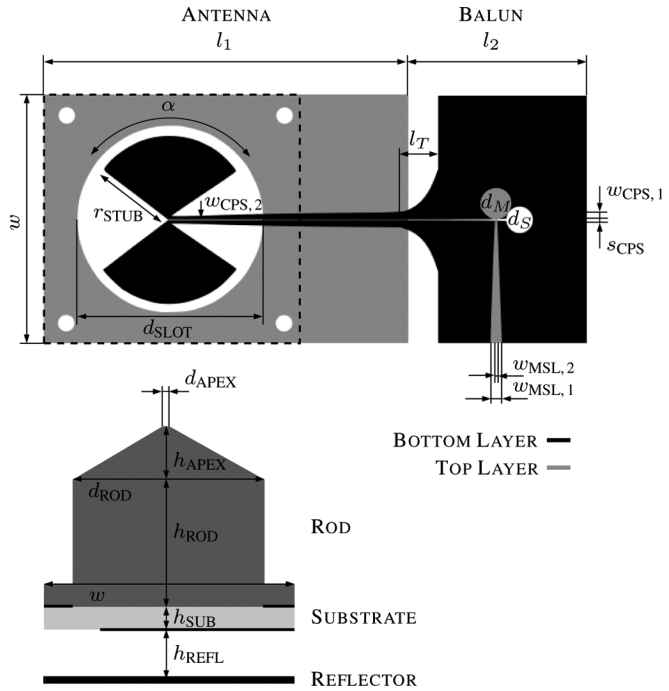

Fig. 2. Sketch of the planar feeding structure including: balun (*top*) and cross section (*bottom*) of the rod together with all design parameters.

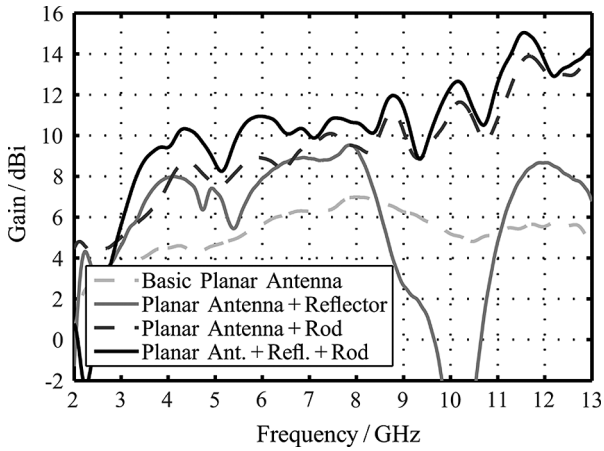

Fig. 3. Simulated gain in main beam direction for different antenna evolution stages assuming lossless materials.

smooth transition to free space and gives a good return-loss behavior. As can be seen in Fig. 3, the gain increases significantly adding the dielectric rod to the basic planar antenna.

Due to the permittivity of the rod with $\varepsilon_r = 2.8$, the electromagnetic fields are mainly concentrated in the dielectric material, in particular at higher frequencies. Therefore, the primarily bidirectional planar antenna now basically radiates in direction of the rod (positive z-direction). In order to further increase the gain and the front-to-back ratio, especially at lower frequencies, a reflector is placed behind the planar antenna. The chosen reflector distance of 14 mm corresponds to $\lambda/4$ at 5.35 GHz and leads to a constructive superposition improving the gain by about 2 dB from 3.1 to 8 GHz. If only the planar antenna together with a reflector are considered, the increased gain at lower frequencies and a decrease at higher frequencies up to

TABLE I
DIMENSIONS OF THE ANTENNA

α	d_{APEX}	d_M	d_{ROD}	d_S
110°	2 mm	5.5 mm	43 mm	4.8 mm
d_{SLOT}	h_{APEX}	h_{REFL}	h_{ROD}	h_{SUB}
33.9 mm	20 mm	14 mm	30 mm	0.8 mm
l_1	l_2	l_T	r_{STUB}	s_{CPS}
99 mm	33 mm	14 mm	14.9 mm	0.3 mm
w	$w_{\mathrm{CPS},1}$	$w_{\mathrm{CPS},2}$	$w_{\mathrm{MSL},1}$	$w_{\mathrm{MSL},2}$
44.8 mm	1 mm	0.48 mm	1.86 mm	0.4 mm

11 GHz due to destructive superposition can be observed (see Fig. 3). This illustrates that the basic planar antenna combined with solely a reflector does not provide a UWB solution.

III. FINAL REALIZATION

All details of the final planar feeding structure including balun for single-ended characterization of the differential antenna and a cross section of the complete dielectric rod antenna are depicted in Fig. 2. The corresponding final dimensions of the design parameters are summarized in Table I. The differentially fed slot and the balun are realized on the microwave substrate RO4003 with a height of 0.8 mm and a permittivity of $\varepsilon_r = 3.38$. The passive balun for measurement purposes consists of two UWB transitions. Firstly, a transition from a coplanar stripline to a slotline applying an exponential taper and, secondly, a slotline-to-microstrip transition. For the second part, a circular-shaped open-circuited stub in microstrip technique and a circular-shaped short-circuited stub in slotline technique are utilized for a broadband operation [28]. An additional tapering of the microstrip line is required to achieve a characteristic impedance of 50 Ω. The impedance of the differential coplanar striplines is 100 Ω being compatible with available integrated circuits. Since the impedance at the antenna feeding point in the center of the slot is slightly higher, a taper is also used for the coplanar stripline.

The dielectric rod is made of polyvinylchlorid (PVC) with a measured permittivity of $\varepsilon_r = 2.8$ and a loss tangent of $\tan\delta = 0.007$. Albeit dielectric materials with a better loss performance are available, the relative dielectric constant of PVC matches well with the substrate material. Furthermore, it is cheap and easily producible. An alternative material for sensors close to strong acids would be polytetrafluoroethylene (PTFE) due to its nonreactive property, but the permittivity of PTFE with $\varepsilon_r = 2.0$ is much lower than that of the substrate.

A photograph of the fabricated antenna is presented in Fig. 4. As can be seen, screws made of polyamide connect the reflector, substrate, and rod with a 3-mm-thick flange. The exact position of the reflector is guaranteed by four polyamide spacers. They stabilize the antenna mechanically and their electrical influence can be neglected as an additional simulation showed. Due to the parasitic radiation by the stubs of the balun, the balun is placed within an aluminum enclosure for shielding purposes. This enclosure is also used as mount for the reflector. Beside the displayed version with a metallic reflector, an antenna without reflector has also been realized. Hence, a PVC plate is used instead

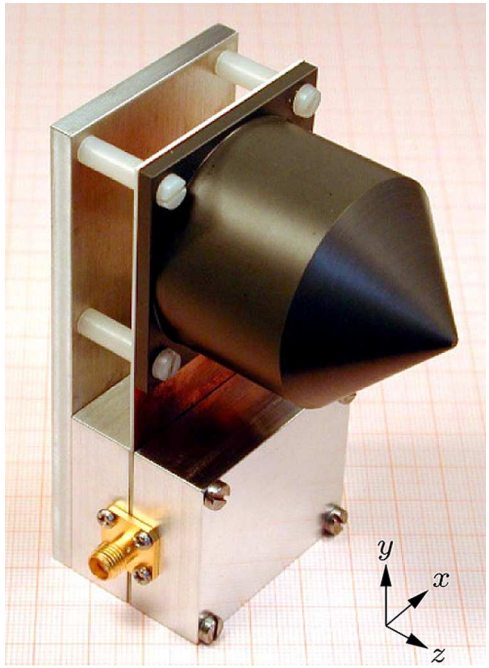

Fig. 4. Photograph of the fabricated UWB rod antenna.

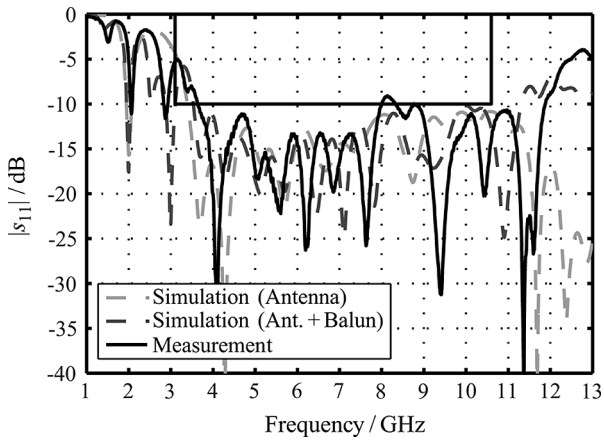

Fig. 5. Simulated and measured reflection coefficient of the rod antenna.

of the reflector. Most of the incident energy penetrates this plate and only about 4% are reflected. Thus, the marginal effects of the metallic reflector on the overall antenna performance can be demonstrated, as will be shown in Section IV.

IV. ANTENNA CHARACTERISTICS

A. Frequency Domain

A common specification in the frequency domain for UWB antennas is a return loss better than 10 dB. This is achieved from 3.5 GHz up to 11.8 GHz for the realized antenna with a minimal violation at 8.1 GHz (see Fig. 5). The observed minor differences between simulation and measurement are caused by the fact that the simulation was performed without the metallic enclosure for the balun. As indicated by the simulation of the antenna without balun, an even wider bandwidth can be achieved by the antenna itself. The balun is the limiting factor, in particular at higher frequencies. At lower frequencies, the balun has

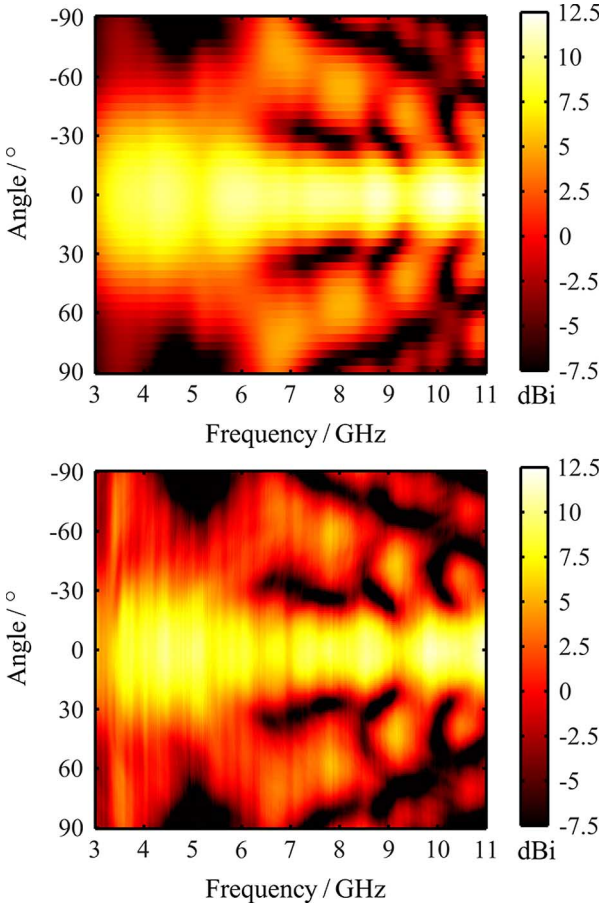

Fig. 6. Simulated (*top*) and measured (*bottom*) radiation pattern for the E-plane (xz-plane) of the UWB rod antenna.

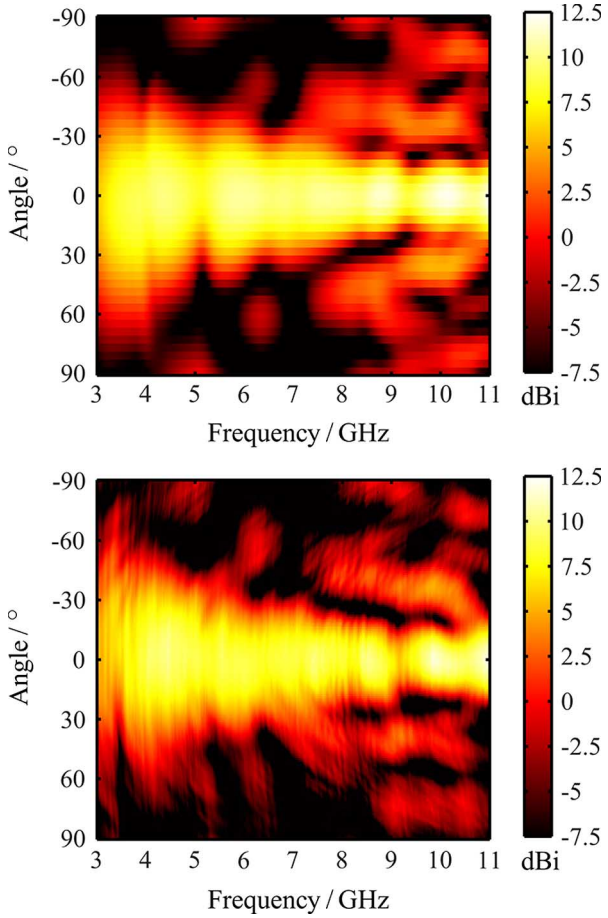

Fig. 7. Simulated (*top*) and measured (*bottom*) radiation pattern for the H-plane (yz-plane) of the UWB rod antenna.

only little effects on the return loss and the reflector mainly leads to a violation of the marked FCC frequency range.

In Figs. 6 and 7, the radiation patterns are shown for the E- and H-plane, respectively. A very good agreement between simulation (including material loss) and measurement is evident. The reason for the undesired sidelobes above 6 GHz in the E-plane is the taper on the circular dielectric waveguide, which acts as a discontinuity and excites a lateral radiation by a leaky wave. A shortened taper, such as proposed in [29], reduces this effect and decreases the sidelobes, but also decreases the return loss. Despite these sidelobes, the beamwidth is quite constant over frequency in both planes. This comes along with a quite constant gain (cf. Fig. 8). The small ripple on the gain over the frequency curve is caused by reflections within the rod. The difference between the simulated and measured gain of about 1 dB is due to the neglected balun in the simulation. As already indicated by Fig. 3, only a marginal gain decrease is measured for the antenna version without a metallic reflector. For the mean gain, calculated in the frequency range from 3 to 11 GHz with [30]

$$G_{\mathrm{mean}}(\theta,\Phi)=\frac{1}{f_2-f_1}\int_{f_1}^{f_2}G(f,\theta,\Phi)\,\mathrm{d}f \qquad (1)$$

only a reduction of 0.7 dB is obtained without the reflector. From the mean gain (see Fig. 9), it can be seen as well that the

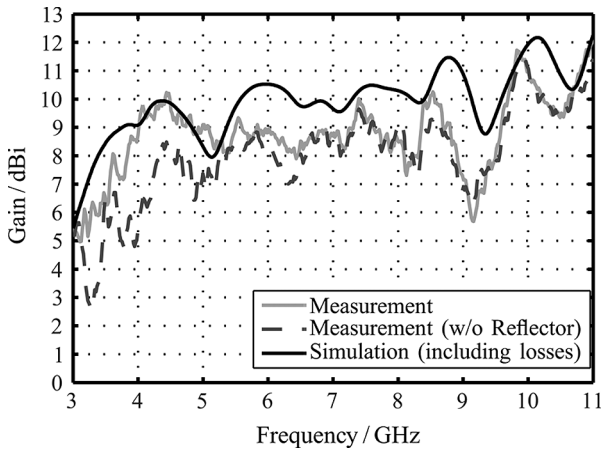

Fig. 8. Gain of the realized antenna in main beam direction versus frequency.

3-dB beamwidth is almost identical for both planes, showing a value of 30° for the H-plane and 31° for the E-plane. Furthermore, the increased sidelobes in the E-plane compared to the H-plane are observable.

As a final characteristic in the frequency domain, Fig. 10 shows the measured cross-polarization isolation for the main beam direction and at the edges of the main beam for both planes. The obtained cross-polarization isolation of better than

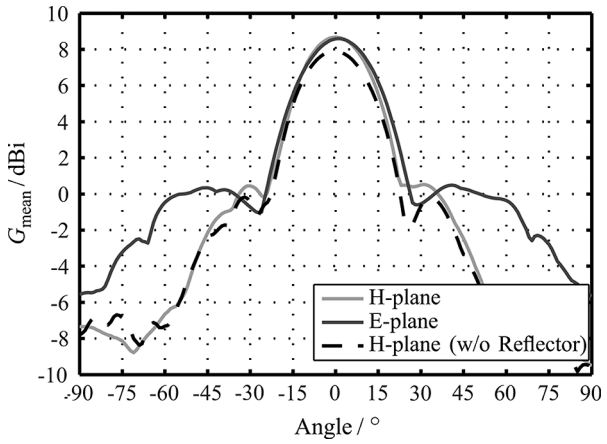

Fig. 9. Mean gain derived from measurements as a function of angle for both planes and without reflector.

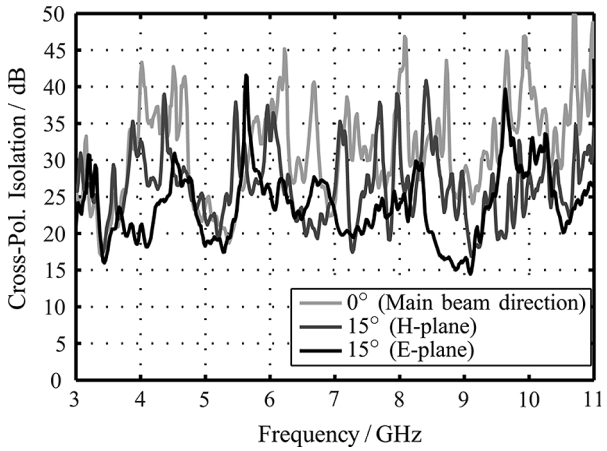

Fig. 10. Measured isolation of the cross polarization for different angles.

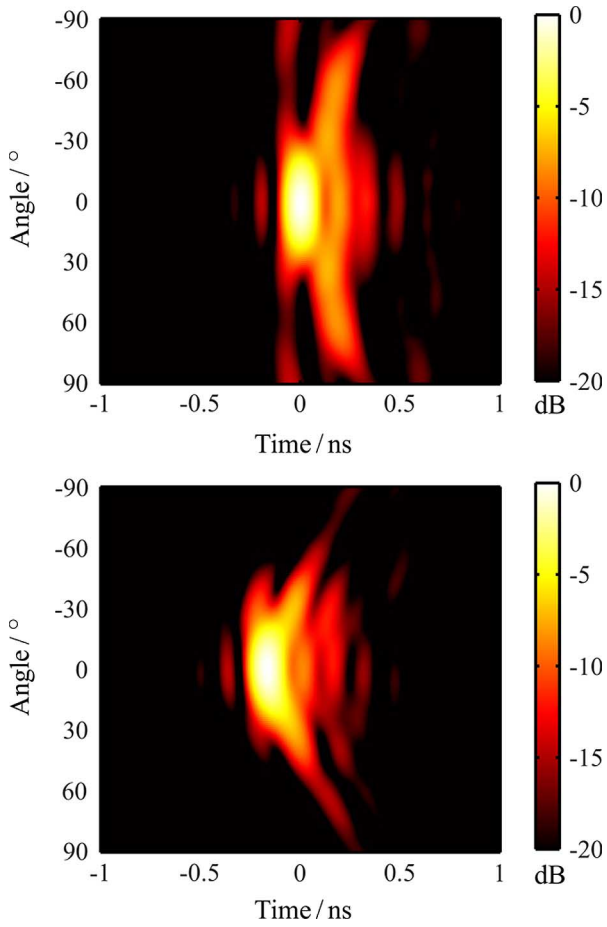

Fig. 11. Normalized envelope of the impulse response obtained by Fourier transform for the: E-plane (*top*) and H-plane (*bottom*) of the measured results.

15 dB within the main beam indicates a good polarization purity for the realized antenna.

B. Time Domain

Impulse-radio UWB systems offer a very simple architecture with low power consumption and low cost in contrast to multi-frequency approaches like multiband orthogonal frequency-division multiplexing (OFDM). Therefore, they are very attractive and currently mainly targeted for the applications described in Section I. For these impulse-based systems, an evaluation of the antenna by the gain information is not sufficient, a small group-delay variation is essential as well. Instead of observing the group delay, the impulse response $h(t)$ is generally considered for all observation angles. The impulse response can be calculated from the complex radiation pattern according to [30] applying the Fourier transform.

Fig. 11 presents the envelope of the calculated impulse responses for both planes normalized to the maximum value of $h_{\max} = 0.55$ m/ns in the logarithmic scale. Similar to the gain in the frequency domain, the impulse response is focused around $\pm 15^{\circ}$, and more importantly, a small impulse width is achieved proving the low-dispersive behavior of the antenna. The figure-of-merit to describe the dispersion performance is the full width at half maximum (FWHM) of the impulse response depicted in Fig. 12 for the E- and H-plane. In the main beam direction, the FWHM is 160 ps. Another characteristic in the time domain is the ringing of the impulse response indicating resonant behavior. The ringing is defined by the time until the absolute value of the impulse response amplitude has fallen below a certain percentage of the impulse response maximum. For the realized antenna, a low ringing of 510 ps is obtained in the main beam direction if a common value of 10% is chosen (cf. Fig. 13).

The description of the antenna characteristics by generic time-domain properties is well suited to compare different antennas, but provides less information on the real system performance. Hence, a direct characterization of the antenna in the time domain has been performed. The results obtained by Fourier transform can then be additionally compared with time-domain measurements. To this end, a UWB impulse generator is connected to the proposed UWB antenna and a free-space transmission measurement is carried out. For the impulse generator, an available monolithically integrated circuit with a fifth-order derivative Gaussian impulse as the output signal has been used [31]. This MMIC is intended to be applied to further sensor realizations. The measured output signal with a peak amplitude of 330 mV is plotted in Fig. 14. The spectrum of this output impulse is conformal with the FCC spectral mask.

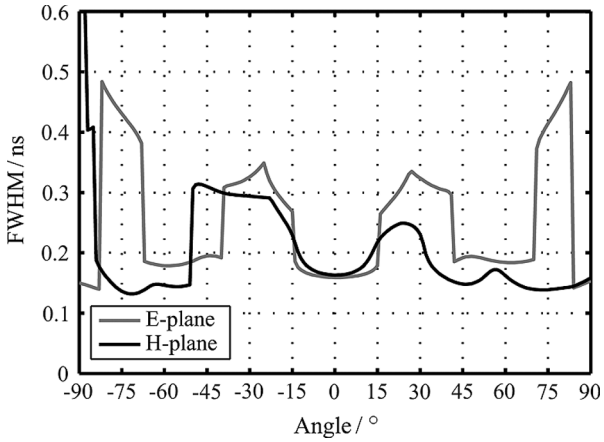

Fig. 12. FWHM for the antenna determined by the impulse responses from Fig. 11.

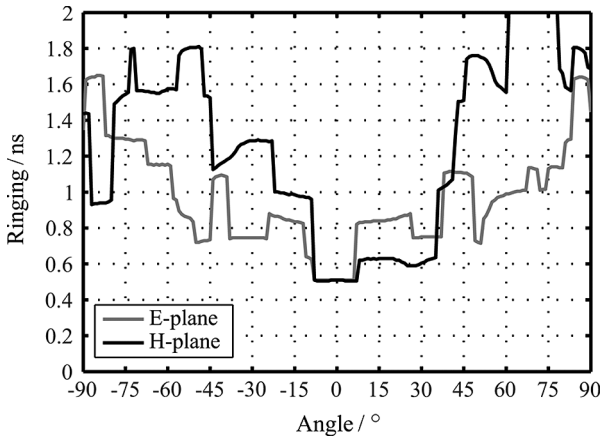

Fig. 13. Ringing performance for the UWB rod antenna for both planes.

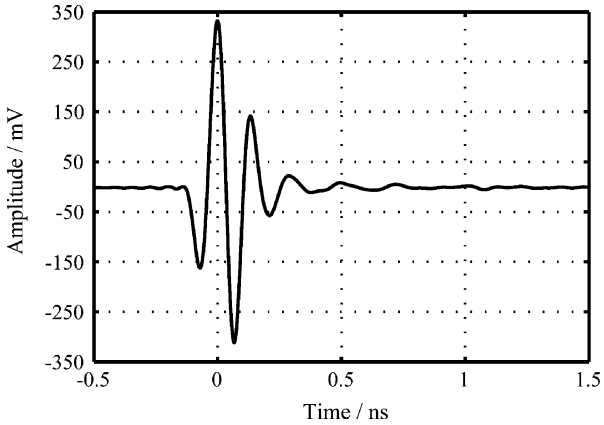

Fig. 14. Output signal of the impulse generator for the time-domain characterization with a fifth-order derivative Gaussian impulse shape.

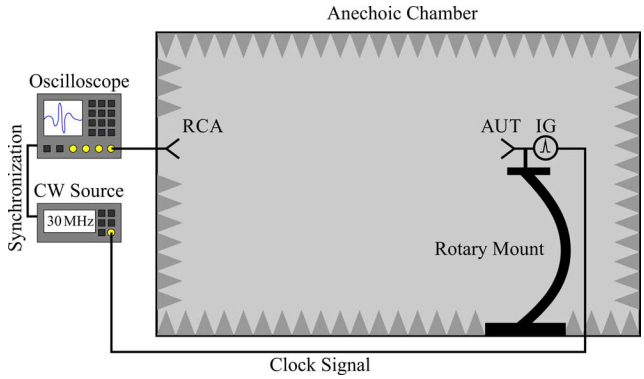

Fig. 15. Measurement setup for the time-domain antenna characterization with receive antenna (RCA), antenna under test (AUT), and impulse generator (IG).

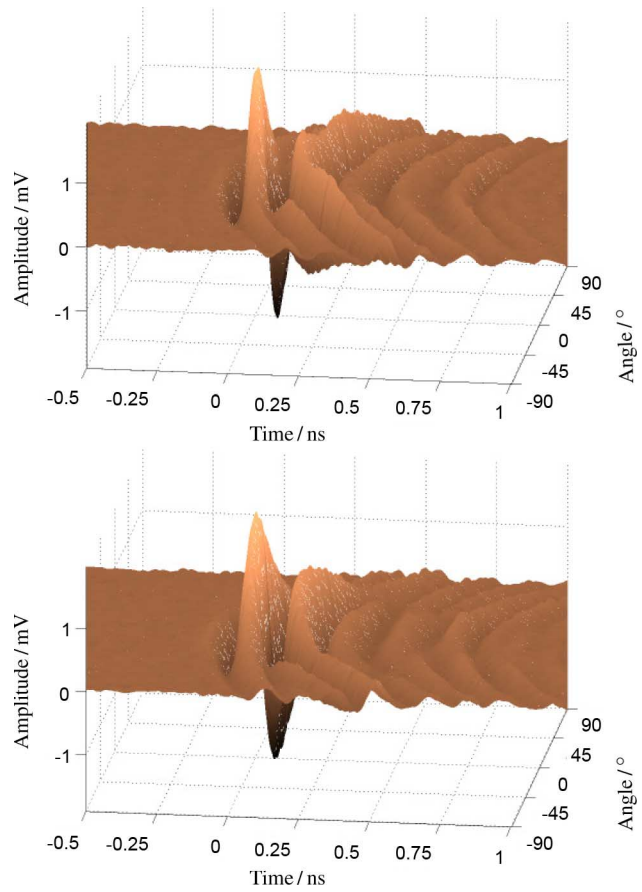

Fig. 16. Measured time domain receive signal for the: E-plane (*top*) and H-plane (*bottom*).

In Fig. 15, the complete measurement setup is sketched. After free-space transmission in an anechoic chamber, the transmitted impulse is captured with a real-time oscilloscope having a suitable bandwidth of 12 GHz. A low-dispersive ridge waveguide horn antenna is employed at the receive side. The trigger signal of the impulse generator is synchronized with the oscilloscope to get the same time base. In this manner, the receive signals are measured for all observation angles of the antenna under test and are presented in Fig. 16 for both planes. A good agreement of these measurements with the impulse responses obtained by the frequency-domain measurements (cf. Fig. 11) can be deduced. Thus, the focus around $\pm 15^{\circ}$ and the broad peak for all angles in the E-plane with an additional delay of approximately 150 ps can be clearly seen. This broad peak is supposed to be caused by the leaky wave leading to the sidelobes in the frequency domain.

For sensing systems, mostly the correlation concept is used at the receiver [7], [12] since the signal-to-noise ratio is maximized if the receive signal is identical to the reference signal. The receiver then acts like an ideal matched filter. An appropriate measure for system characterization in case of a

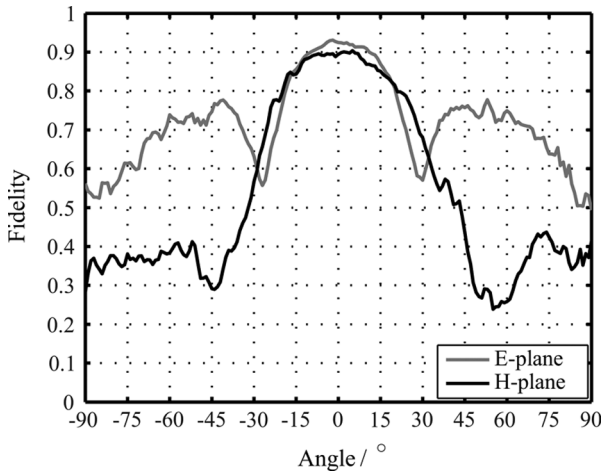

Fig. 17. Fidelity factor for both planes calculated with (2) from Fig. 16.

TABLE II
COMPARISON OF DIFFERENT UWB ROD ANTENNAS

	TSA Rod [24]	Dipole Rod [25]	This work
Dimensions / cm	$6.8 \times 9.3 \times 9.8$	$20 \times 20 \times 8.5$	$4.4 \times 4.6 \times 7$
$\lvert s_{11}\rvert < -5$ dB	2.5 – 8.5 GHz	2.7 – 20 GHz	2.7 – 12.5 GHz
$\lvert s_{11}\rvert < -10$ dB	—	3 – 16 GHz	3.5 – 11.8 GHz
G_{mean} / dBi	9.0	8.9	8.7
$h_{\max}$ / $\frac{\text{m}}{\text{ns}}$	0.69	0.69	0.55
FWHM / ps	170	230	160
Ringing / ps	445	540	510

correlation receiver is the fidelity F defined as [32]

$$F = \max_{\tau} \left(\frac{\int_{-\infty}^{\infty} s_{\text{REF}}(t) \cdot s_{\text{RX}}(t+\tau)\, \text{d}t}{\int_{-\infty}^{\infty} |s_{\text{REF}}(t)|^2\, \text{d}t \int_{-\infty}^{\infty} |s_{\text{RX}}(t)|^2\, \text{d}t} \right). \quad (2)$$

A fidelity of $F = 1$ indicates no signal disturbance and a maximum system performance for the correlation receiver. Fig. 17 presents the fidelity obtained from the measurement results in Fig. 16 if the reference signal s_{REF} is identical to the transmit impulse, which is typically true for correlation receivers.

Within the main beam of the antenna, a fidelity of at least $F = 0.85$ is achieved proving a very good system performance of the presented UWB rod antenna in combination with the applied impulse generator. In contrast to the frequency-domain results, the insignificant dispersive influences of the receive antenna are still included in this result. In the E-plane, an increased fidelity around $\pm 50^\circ$ due to the leaky wave can be identified.

V. CONCLUSION

The highly directional UWB rod antenna presented in this paper exhibits a UWB performance and a low dispersive behavior, as shown by the time-domain measurements. The return loss of the antenna is better than 10 dB from 3.5 to 11.8 GHz, where the balun is the limiting factor for the upper frequency. An even wider bandwidth can be expected without a balun, and hence, a similar bandwidth is feasible such as for the rod antenna in [24]. Within the FCC frequency range, a flat gain is achieved with a mean gain of 8.7 dBi. The comparison of this antenna with recently reported UWB antennas also based on a dielectric rod is given in Table II and shows a high directionality in relation to the antenna size for this work. Furthermore, the good time-domain behavior is expressed by this comparison since a reasonable ringing is obtained and the impulse width of 160 ps outperforms the previously published antennas. The suitability for impulse-based UWB systems is demonstrated additionally by the separately performed time-domain characterization applying an FCC compliant impulse.

Besides the good electrical properties, this planar fed rod antenna offers a very simple assembly, low fabrication cost, and a high integration level in combination with active circuits with a very compact size. This makes the antenna very attractive for various modern UWB sensing applications. Additionally, the basic antenna concept features the flexibility to change the dielectric rod material, the base substrate, or even the planar feeding structure. Thus, the antenna can be adopted easily to a specific environment. For instance, an unbalanced UWB slot antenna [33] instead of the differential structure could be used if single-ended active circuits are preferred in the sensor design.

ACKNOWLEDGMENT

The authors would like to thank the UWB working group of Prof. H. Schumacher, Institute of Electron Devices and Circuits, University of Ulm, Ulm, Germany, for providing the impulse generator.

REFERENCES

[1] "Revision of part 15 of the Commission's rules regarding ultra-wideband transmission systems," FCC, Washington, DC, First Rep. and Order 48-02, Apr. 2002.
[2] G. Stickley, I. Longstaff, and M. Radcliffe, "Synthetic aperture radar for the detection of shallow buried objects," in *EUREL Int. Detection Abandoned Land Mines Conf.*, Oct. 1996, vol. 431, pp. 160–163.
[3] S. Vitebskiy, L. Carin, M. A. Ressler, and F. H. Le, "Ultra-wideband, short-pulse ground-penetrating radar: Simulation and measurement," *IEEE Trans. Geosci. Remote Sens.*, vol. 35, no. 3, pp. 762–772, May 1997.
[4] E. Zaikov, J. Sachs, M. Aftanas, and J. Rovnakova, "Detection of trapped people by UWB radar," in *German Microw. Conf.*, Mar. 2008, pp. 240–243.
[5] T. McEwan and S. Azevedo, "Micropower impulse radar," *Sci. Technol. Rev.*, pp. 16–29, Jan. 1996.
[6] S. Hantscher, A. Reisenzahn, and C. G. Diskus, "An UWB wall scanner based on a shape estimating SAR algorithm," in *IEEE MTT-S Int. Microw. Symp. Dig.*, Jun. 2007, pp. 1463–1466.
[7] J. Huettner, R. Gierlich, A. Ziroff, and R. Weigel, "A low cost ultra-wide-band pulse radar in a guided wave gauging application," in *Eur. Radar Conf.*, Sep. 2009, pp. 101–104.
[8] A. W. Hees, "UWB-Radarsensor zur Unterscheidung zwischen menschlichem Gewebe und Werkstoffen," Tech. Univ. München, Munich, Germany, 2009.
[9] X. Li, E. J. Bond, B. D. Van Veen, and S. C. Hagness, "An overview of ultra-wideband microwave imaging via space-time beamforming for early-stage breast-cancer detection," *IEEE Trans. Antennas Propag.*, vol. 47, no. 1, pp. 19–34, Feb. 2005.
[10] M. Klemm, I. J. Craddock, J. A. Leendertz, A. Preece, and R. Benjamin, "Radar-based breast cancer detection using a hemispherical antenna array," *IEEE Trans. Antennas Propag.*, vol. 57, no. 6, pp. 1692–1704, Jun. 2009.
[11] E. M. Staderini, "UWB radars in medicine," *IEEE Aerosp. Electron. Syst. Mag.*, vol. 17, no. 1, pp. 13–18, Jan. 2002.
[12] M. Leib, W. Menzel, B. Schleicher, and H. Schumacher, "Vital signs monitoring with a UWB radar based on a correlation receiver," in *Eur. Antennas Propag. Conf.*, Apr. 2010, pp. 1–5.

[13] F. Thiel, M. Hein, U. Schwarz, J. Sachs, and F. Seifert, "Fusion of magnetic resonance imaging and ultra-wideband-radar for biomedical applications," in *IEEE Int. Ultra-Wideband Conf.*, Sep. 2008, vol. 1, pp. 97–100.
[14] P. J. Gibson, "The Vivaldi aerial," in *Eur. Microw. Conf.*, Oct. 1979, pp. 101–105.
[15] U. Schwarz, F. Thiel, F. Seifert, R. Stephan, and M. Hein, "Magnetic resonance imaging compatible ultra-wideband antennas," in *Eur. Antennas Propag. Conf.*, Mar. 2009, pp. 1102–1105.
[16] J. Bourqui, E. C. Fear, and M. Okoniewski, "Versatile ultrawideband sensor for near-field microwave imaging," in *Eur. Antennas Propag. Conf.*, Apr. 2010, pp. 1–5.
[17] Y. Yang, C. Zhang, S. Lin, and A. E. Fathy, "Development of an ultra wideband Vivaldi antenna array," in *IEEE Int. Antennas Propag. Symp.*, Jul. 2005, vol. 1A, pp. 606–609.
[18] C. T. Rodenbeck, S.-G. Kim, W.-H. Tu, M. R. Coutant, S. Hong, M. Li, and K. Chang, "Ultra-wideband low-cost phased-array radars," *IEEE Trans. Microw. Theory Tech.*, vol. 53, no. 12, pp. 3697–3703, Dec. 2007.
[19] M. Klemm and G. Tröster, "Characterisation of an aperture-stacked patch antenna for ultra-wideband wearable radio systems," *J. Telecommun. Inform. Technol.*, vol. 2, pp. 39–44, 2005.
[20] M. Frei, M. Leib, and W. Menzel, "A symmetrically fed aperture-coupled stacked-patch antenna," in *IEEE Int. Antennas Propag. Symp.*, Jun. 2009, pp. 1–4.
[21] M. Ameya, M. Yamamoto, T. Nojima, and K. Itoh, "Leaf-shaped element bowtie antenna with flat reflector for UWB applications," *IEICE Trans. Commun.*, vol. 90 B, no. 9, pp. 875–884, Sep. 2007.
[22] Y. Ranga, K. P. Esselle, A. Weily, and A. K. Verma, "A compact antenna with high gain for ultra wide band systems," in *Eur. Microw. Conf.*, Oct. 2009, pp. 85–88.
[23] A. Hees, J. Hasch, and J. Detlefsen, "Characteristics of a corrugated tapered slot antenna with dielectric rod and metallic reflector," in *IEEE Int. Ultra-Wideband Conf.*, Sep. 2008, vol. 1, pp. 1–4.
[24] M. D. Blech and T. F. Eibert, "A dipole excited ultrawideband dielectric rod antenna with reflector," *IEEE Trans. Antennas Propag.*, vol. 55, no. 7, pp. 1948–1954, Jul. 2007.
[25] Microwave Studio. Comput. Simulation Technol. (CST), Darmstadt, Germany, 2009.
[26] M. Leib, M. Frei, and W. Menzel, "A novel ultra-wideband circular slot antenna excited with a dipole element," in *IEEE Int. Ultra-Wideband Conf.*, Sep. 2009, pp. 386–390.
[27] T. W. Hertel, "Cable-current effects of miniature UWB antennas," in *IEEE Int. Antennas Propag. Symp.*, Jul. 2005, vol. 3A, pp. 524–527.
[28] B. Schueppert, "Microstrip/slotline transitions: Modeling and experimental investigation," *IEEE Trans. Microw. Theory Tech.*, vol. 36, no. 8, pp. 1272–1282, Aug. 1988.
[29] G. Adamiuk, T. Zwick, and W. Wiesbeck, "Compact, dual-polarized UWB-antenna, embedded in a dielectric," *IEEE Trans. Antennas Propag.*, vol. 58, no. 2, pp. 279–286, Feb. 2010.
[30] W. Sörgel and W. Wiesbeck, "Influence of the antennas on the ultra-wideband transmission," *EURASIP J. Appl. Signal Process.*, vol. 3, pp. 296–305, 2005.
[31] J. Dederer, B. Schleicher, F. De Andrade Tabarani Santos, A. Trasser, and H. Schumacher, "FCC compliant 3.1–10.6 GHz UWB pulse radar using correlation detection," in *IEEE MTT-S Int. Microw. Symp. Dig.*, Jun. 2007, pp. 1471–1474.
[32] D.-H. Kwon, "Effect of antenna gain and group delay variations on pulse-preserving capabilities of ultrawideband antennas," *IEEE Trans. Antennas Propag.*, vol. 54, no. 8, pp. 2208–2215, Aug. 2006.
[33] E. S. Angelopoulos, A. Anastopoulos, D. I. Kaklamani, A. A. Alexandridis, F. Lazarakis, and K. Dangakis, "Circular and elliptical CPW-fed slot and microstrip-fed antennas for ultrawideband applications," *IEEE Antennas Wireless Propag. Lett.*, vol. 5, no. 1, pp. 294–297, Dec. 2006.

Mario Leib (S'05) received the Dipl.-Ing. degree in electrical engineering and Dr.-Ing. degree from the University of Ulm, Ulm, Germany, in 2004 and 2011, respectively.

From 2004 to 2010, he was with the Institute of Microwave Techniques, University of Ulm. Since 2011, he has been with EADS Deutschland GmbH, Ulm, Germany. His main research topics are UWB antennas, components, and radar sensors.

Andreas Vollmer was born in Freiburg, Germany, in 1981. He received the Dipl.-Ing. degree in electrical engineering from the University of Ulm, Ulm, Germany, in 2010. His diploma thesis concerned UWB antennas and arrays with high directivity.

His diploma thesis was performed at the Institute of Microwave Techniques, University of Ulm. In 2010, he joined Emitel AG, Ulm, Germany.

Wolfgang Menzel (M'89–SM'90–F'01) received the Dipl.-Ing. degree in electrical engineering from the Technical University of Aachen, Aachen, Germany, in 1974, and the Dr.-Ing. degree from the University of Duisburg, Duisburg, Germany, in 1977.

From 1979 to 1989, he was with the Millimeter-Wave Department, AEG, (now EADS, European Aeronautic Defence and Space Company), Ulm, Germany, where he headed the entire Millimeter-Wave Department from 1985 to 1989. In 1989, he became a Full Professor with the Institute of Microwave Techniques, University of Ulm, Ulm, Germany. His current areas of interest are multilayer planar circuits, antennas, millimeter-wave and microwave interconnects and packaging, and millimeter-wave sensors.

Prof. Menzel was an associate editor for the IEEE TRANSACTIONS ON MICROWAVE THEORY AND TECHNIQUES (2003–2005). From 1997 to 1999, he was a Distinguished Microwave Lecturer for Microwave/Millimeter Wave Packaging. From 1997 to 2001, he chaired the German IEEE Microwave Theory and Techniques (MTT)/Antennas and Propagation (AP) Chapter. He was the recipient of the 2002 European Microwave Prize.